



Least-Squares-Based Reaction Control of Space Manipulators

Silvio Cocuzza,* Isacco Pretto,† and Stefano Debei‡
University of Padova, 35131 Padova, Italy

DOI: 10.2514/1.45874

This paper presents a novel solution for the inverse kinematics of redundant space manipulators, which is aimed at locally minimizing the dynamic disturbances transferred to the spacecraft during trajectory tracking maneuvers. The solution is based on a constrained least-squares approach and is suitable for real-time implementation. To formulate the problem as a function of dynamic variables, the inverse kinematics at the acceleration level is considered. The proposed solution is introduced in the context of a more general theory, including the classical pseudoinverse, the extended task-space, and the task priority solutions. Moreover, the introduction of joint acceleration constraints in order to take into account the physical limits of the manipulator joints and the relaxing of the end-effector tracking requirements have been studied, and their influence on the minimization performance has been assessed. The experimental validation of the proposed solutions, with an insight on the effect of joint flexibility on their performance, has been carried out for a planar three-degrees-of-freedom manipulator. Two test cases have been considered, in which the number of force and torque reaction components to be controlled are equal to or greater than the available degree of redundancy.

Nomenclature

D	= diameter of circular trajectory, m
e	= end-effector pose error, m or rad
F	= force, N
f	= cost function
f_n	= joint first eigenfrequency, Hz
I	= identity matrix
$I_{Gx}, I_{Gy},$ I_{Gz}	= link principal moments of inertia about the center of mass, kg · m ²
I_s	= spacecraft inertia tensor, kg · m ²
J, Z	= manipulator Jacobian matrix and null-space projector
k, d	= components of end-effector pose and base reaction to be controlled
k_m	= mass ratio
l, l_G	= robot link length and distance of link center of mass from previous joint axis, m
M, n	= mass matrix and centrifugal and Coriolis term
m, m_A, m_s	= robot link mass, robotic arm mass, and spacecraft mass, kg
m_a, m_p	= variable robotic arm mass and payload mass, kg
n, r	= degrees of freedom and degree of redundancy of manipulator
n_{\lim}, r_{eff}	= number of active joint acceleration limits and effective degree of redundancy
PI	= performance indicator, %
q	= joint variables of manipulator, rad or m
$^w R$	= weighted reaction
r_s	= spacecraft position, m
T	= torque, N · m
t	= time, s
W	= weight matrix
w	= term of weight matrix, N ⁻¹ or (N · m) ⁻¹

Received 8 June 2009; revision received 14 January 2010; accepted for publication 10 February 2010. Copyright © 2012 by Silvio Cocuzza. Published by the American Institute of Aeronautics and Astronautics, Inc., with permission. Copies of this paper may be made for personal or internal use, on condition that the copier pay the \$10.00 per-copy fee to the Copyright Clearance Center, Inc., 222 Rosewood Drive, Danvers, MA 01923; include the code 0731-5090/12 and \$10.00 in correspondence with the CCC.

*Research Associate, Center of Studies and Activities for Space “G. Colombo”, Via Venezia 15; silvio.cocuzza@unipd.it. Member AIAA.

†Ph.D. Student, Center of Studies and Activities for Space “G. Colombo”, Via Venezia 15; isacco.pretto@unipd.it. Student Member AIAA.

‡Associate Professor, Department of Mechanical Engineering, Via Venezia 1; stefano.debei@unipd.it.

x, x_d	= actual and desired end-effector pose, m or rad
δ	= reaction error, N, N · m, or dimensionless
ζ	= joint rotational damping ratio
λ_x, λ_R	= weight factor for end-effector pose error and for weighted reaction
μ	= ratio between end-effector and weighted reaction weight factors
$\dot{\phi}, \ddot{\phi}$	= arbitrary vectors in joint velocity and acceleration spaces
ω_s	= spacecraft angular velocity, rad/s

Subscripts

B, C	= base spacecraft and attitude control system
F, T	= force and torque
IKS	= inverse kinematics solution: least-squares solution, least-squares solution with equality constraints, or least-squares solution with equality and inequality constraints
l, u	= lower and upper limits
R, x, λ	= weighted reaction, end-effector pose error, and weighted combination of them
tot, flex,	= total, due to joint flexibility, and due to not modeled effects
mod	
∞, k, exp	= rigid joints simulation, flexible joints simulation, and experimental measure

I. Introduction

SPACE manipulators during operations transfer reaction forces and torques to the base spacecraft due to their motion, which may cause undesired attitude changes. In this paper, inverse kinematics (IK) redundancy resolution schemes based on a constrained least-squares (CLS) approach are introduced, which are aimed at locally minimizing the dynamic disturbances transferred to the spacecraft during trajectory tracking maneuvers of kinematically redundant manipulators. The minimization of these disturbances is important in order to 1) maintain the antennas communication link, the orientation of pointing instrumentation, and scanning devices. Reduced dynamic disturbances result in a reduced energy consumption of the attitude control system (ACS) for the maintenance of the desired attitude [1–3], or for the reorientation after the manipulator maneuver, and therefore lead to an increased system useful life; 2) in order to preserve the microgravity environment onboard the spacecraft [4]; and 3) in order to reduce the energy consumption of the propulsion system, if a controlled spacecraft position is required.

A number of redundancy resolution schemes have been proposed according to a kinematic approach, for the local minimization of the spacecraft angular velocity, exploiting the momentum and angular momentum conservation laws [5,6]. In particular, robot motions, if any, which allow to maintain the same spacecraft attitude can be found by means of the fixed attitude restricted Jacobian matrix [7]. Heuristic path planning methods, from which a disturbance map is derived [8,9], have also been proposed. The utilization of the nonholonomic properties of the system in the path planning problem has been pointed out in [10,11]. On the other hand, other authors proposed a dynamic approach, which is also used in this paper, for which the aim is to reduce the reactions transferred to the base spacecraft. A local optimization approach for reaction minimization was proposed in [12,13], in which a Rayleigh–Ritz technique and polynomial shape functions are used in order to determine the joint trajectories. A Lagrangian constrained optimization method has been proposed in [14,15], in which second- and fourth-order polynomials are used in order to approximate the base motion. The reaction null-space (RNS) concept [16,17] has been proposed in order to study the existence of zero reaction paths in the manipulator workspace. Recently, an optimization method based on a weighted pseudoinversion of the Jacobian matrix [18] has been proposed. Globally optimal solutions [13] outperform local ones but require heavy computations that rule out real-time control.

The solution proposed in this paper has to be considered in the framework of local optimization methods, in which the Jacobian of a redundant system is inverted while taking an optimality constraint into account. A brief literature review on this topic follows, which will be useful to show how this work fits within it.

In the case of nonredundant manipulators ($n = k$), the resolved motion rate control (RMRC) [19] and the resolved acceleration control (RAC) [20] have been extensively used. The RMRC uses a formulation of the IK problem at the velocity level:

$$\dot{\mathbf{x}} = \mathbf{J}\dot{\mathbf{q}} \quad (1)$$

where $\dot{\mathbf{x}}$ is given, and $\dot{\mathbf{q}}$ can be computed by inverting the equation. On the other hand, the RAC uses a formulation of the IK at the acceleration level:

$$\ddot{\mathbf{x}} - \mathbf{J}\dot{\mathbf{q}} = \mathbf{J}\ddot{\mathbf{q}} \quad (2)$$

where $\ddot{\mathbf{x}}$ is given, and $\dot{\mathbf{q}}$ is computed; therefore, the equation can be solved for $\ddot{\mathbf{q}}$ in a similar way as Eq. (1). In the nonredundant case, \mathbf{J} is a square matrix and, if it is full rank, can be directly inverted.

In the redundant case ($n > k$), several methods have been proposed for solving Eq. (1) [which can also be straightforwardly applied to Eq. (2)] while taking into account a given performance criterion. According to the classification proposed in [21,22], these methods solve the redundancy by means of 1) a particular solution of Eq. (1), which uses a generalized inverse [19,21,23,24], generally the Moore–Penrose pseudoinverse [19]; 2) the general solution of Eq. (1), expressed in terms of a generalized inverse of \mathbf{J} , which can be represented as the sum of any particular solution and the general solution of the homogeneous equation $\mathbf{J}\dot{\mathbf{q}} = \mathbf{0}$ [25]:

$$\dot{\mathbf{q}} = \mathbf{J}^{-}\dot{\mathbf{x}} + (\mathbf{I} - \mathbf{J}^{-}\mathbf{J})\dot{\phi} \quad (3)$$

in which the arbitrary vector $\dot{\phi}$ has to be determined in order to obtain the optimization of one or more performance criteria; and 3) a nonredundant system, by adjoining one or more performance criteria to the kinematic equations, such as proposed in the extended task-space (ETS) technique [21,26,27].

In case that the general solution of Eq. (1) is used, the arbitrary vector can be determined by using different techniques, most of which can be reduced to the gradient projection technique [25] and the task priority (TP)-based redundancy control method [28].

The aforementioned redundancy resolution methods have been applied to various performance criteria, such as obstacle avoidance [28,29], singularity avoidance [24,27], joint-limit avoidance [25], minimization of joint velocities [19], accelerations, torques [30],

power consumption [31], and minimization of kinetic energy [32], and to multicriteria optimization [21]. A unified framework for many velocity-control techniques, which allows efficient and accurate implementation, has been proposed in [33].

All the redundancy resolution methods that are derived for fixed-based manipulators can be straightforwardly applied to free-floating robots by considering the free-floating base kinematic and dynamic models instead of the fixed-based ones [34].

In the solution proposed in this paper, in which the IK is formulated at the acceleration level and the performance criterion is related to the minimization of base reactions, the problem statement is identified as a least-squares problem with equality constraints (LSE), which can be directly solved in real time [35–41] with no need of any explicit inversion of Eq. (2) through a generalized inverse. A closed-form solution has also been derived, which is equivalent to the one that can be derived by applying the TP method expressed at the acceleration level and in which the trajectory tracking task is given the first priority and the reaction minimization task is given the second priority. Moreover, a different formulation of the solution has been derived in the framework of the ETS technique by using the weighting method [42–44], which allows the kinematic equation to be exactly satisfied and the performance criterion to be minimized in a least-squares (LS) sense (such as in the TP formulation). An interesting result is that the use of increasing weights makes the ETS solution approach the TP one. The use of the weighting method in this context has several advantages:

- 1) Simple real-time LS routines can be used for the solution.
- 2) It can be easily extended to multicriteria optimization, with the possibility to give a different weight to each criterion.
- 3) The minimization performance can be enhanced by relaxing the end-effector (EE) tracking requirements (see Sec. IV.B).

The main contributions of the present work, which are original to the best of authors' knowledge, are as follows: 1) the introduction of a CLS-based redundancy resolution scheme for the local minimization of base reactions, which is suitable for real-time solution; 2) the introduction of the proposed solution in a more general theory, including the classical pseudoinverse solution, the ETS solution, and the TP solution; 3) the introduction of joint acceleration constraints in order to take into account the physical limits of the manipulator joints, and the study of their influence on the minimization performance; and 4) the study of the performance and the experimental validation of the presented IK solutions for two test cases ($r < d$ and $r = d$). In the second test case, a zero reaction solution has been found, which is not possible in the first test case.

The paper is organized as follows: Sec. II presents the advantages of the proposed solution and possible operating scenarios, Sec. III introduces the formulation of the problem, Sec. IV presents the novel IK solutions, Sec. V describes the experimental setup, Sec. VI presents the simulation and experimental results, and Sec. VII concludes the paper.

II. Operating Scenarios and Advantages of the Proposed Solution

In the operating scenario of a target approach maneuver, the free-floating mode (i.e., manipulation with the ACS and the propulsion system turned off) is more adequate than the free-flying mode (ACS and propulsion system on) in the final approach phase, both because it leads to more accurate EE positioning [3] and for safety reasons. On the other hand, in the target coarse approach maneuver, a low disturbance motion should be used together with the ACS turned on in order to reduce the time for the maneuver and for the recovery of the desired attitude [3]. In this way, the risk of approaching the boundary of the manipulator workspace is also reduced. Another possibility is to use the coordinated control of the manipulator and base attitude by means of angular momentum feed-forward compensation [2,45,46].

In this context, the use of a dynamic approach presents the following advantages with respect to a kinematic approach:

- 1) The ACS energy consumption when the manipulation is carried out with controlled attitude can be reduced (for example, in the target

coarse approach phase [3]), because the dynamic disturbances to be compensated with the ACS are directly minimized;

2) Both the forces and torques transferred to the spacecraft can be minimized, thus preserving the onboard microgravity environment;

3) The energy consumption of the propulsion system can be reduced if a controlled spacecraft position is required during the manipulation or if the initial position (with respect to the serviced spacecraft or the International Space Station) has to be recovered after the manipulation in order to perform another task.

On the other hand, if the manipulation is carried out with the ACS turned off (for example, in the fine manipulation phase), the use of a kinematic approach is more adequate than a dynamic approach because it leads to minimum attitude changes, and therefore to minimum energy consumption for the spacecraft reorientation after the manipulation maneuver.

To perform a reactionless manipulation (computed, for example, using the RNS concept [16,17]), a sufficient number of degrees of freedom (DOF) with respect to the task variables of the spacecraft task and EE task are necessary [5]. Moreover, it is possible to perform reactionless manipulations only in a reduced workspace [7]. The redundancy resolution scheme presented in this paper overcomes these limitations because it exploits the redundancy in order to minimize the base reactions, giving the same RNS solution when sufficient DOF are available.

In comparison with previous dynamic formulations [12–15,18], the one presented in this paper has the advantage of the simplicity of the mathematical formulation (see Sec. IV), the need of standard LS routines for the solution, which are suitable for real-time implementation [35–41], and the possibility to take into account the physical limits of the manipulator joints (see Sec. IV.D).

III. Problem Formulation

Consider a redundant manipulator tracking a desired EE trajectory $\mathbf{x}_d = \mathbf{x}_d(t)$. In accordance with the approach used in previous works [12,13,15], a suitable measure for the base reaction is the weighted quadratic cost function f_R , which is defined by means of a weighted combination of the base reaction forces and torques:

$$f_R \triangleq (^w\mathbf{R})^T \cdot (^w\mathbf{R}) = \| ^w\mathbf{R} \|^2 \quad (4)$$

in which the weighted reaction ${}^w\mathbf{R}$ is defined as

$${}^w\mathbf{R} \triangleq \mathbf{W} \begin{bmatrix} \mathbf{F}_B \\ \mathbf{T}_B \end{bmatrix} = \begin{bmatrix} \mathbf{W}_F & \mathbf{0} \\ \mathbf{0} & \mathbf{W}_T \end{bmatrix} \begin{bmatrix} \mathbf{F}_B \\ \mathbf{T}_B \end{bmatrix} \quad (5)$$

The weight matrix \mathbf{W} is a positive definite diagonal matrix, which takes into account the relative importance of each reaction component and the dimensional incompatibility that exists between forces and torques.

A. Base Reaction Dynamics

Taking into account the attitude disturbance, the time evolution of the spacecraft angular velocity $\boldsymbol{\omega}_s$ during a manipulator maneuver is mainly due to the ACS torque \mathbf{T}_C and to the reaction torque \mathbf{T}_B generated by the manipulator, as expressed by the Euler equation that, evaluated with respect to a spacecraft-fixed reference frame, becomes [47]

$$\mathbf{T}_B + \mathbf{T}_C = \mathbf{I}_s \dot{\boldsymbol{\omega}}_s + \boldsymbol{\omega}_s \times \mathbf{I}_s \boldsymbol{\omega}_s \quad (6)$$

where \mathbf{T}_B , \mathbf{T}_C , and \mathbf{I}_s are evaluated with respect to the spacecraft center of mass (cm).

On the other hand, the time evolution of the spacecraft cm position is due to the reaction force \mathbf{F}_B and to the thrust \mathbf{F}_C eventually generated by the ACS or by the propulsion system, as expressed by the equation of Newton:

$$\mathbf{F}_B + \mathbf{F}_C = m_s \ddot{\mathbf{r}}_s \quad (7)$$

The inverse dynamics of \mathbf{T}_B can be expressed as a second-order dynamic system [13]:

$$\mathbf{T}_B = \mathbf{M}_T \ddot{\mathbf{q}} + \mathbf{n}_T \quad (8)$$

Similarly, \mathbf{F}_B can be expressed as

$$\mathbf{F}_B = \mathbf{M}_F \ddot{\mathbf{q}} + \mathbf{n}_F \quad (9)$$

Finally, according to its definition, the general inverse dynamics of ${}^w\mathbf{R}$ can be expressed as[§]

$${}^w\mathbf{R} = \mathbf{M} \ddot{\mathbf{q}} + \mathbf{n} \quad (10)$$

where the mass matrix is defined as

$$\mathbf{M} \triangleq \mathbf{W} \begin{bmatrix} \mathbf{M}_F \\ \mathbf{M}_T \end{bmatrix}$$

and the centrifugal and Coriolis term is defined as

$$\mathbf{n} \triangleq \mathbf{W} \begin{bmatrix} \mathbf{n}_F \\ \mathbf{n}_T \end{bmatrix}$$

The mass matrix depends on \mathbf{q} , whereas the centrifugal and Coriolis term depends on \mathbf{q} and $\dot{\mathbf{q}}$ [13]. Moreover, for a very massive spacecraft, the system dynamics approaches the one of a fixed-based manipulator [34].

B. Base Reaction Minimization

In this section, an optimization problem is defined in order to obtain the IK solution that minimizes the cost function f_R . Since the dynamics of ${}^w\mathbf{R}$ is expressed by means of a second-order differential system [Eq. (10)], a second-order differential kinematic approach is used, in which $\ddot{\mathbf{q}}$ can be regarded as the local optimization variable. The forward kinematics (FK) equation relates the EE trajectory and the trajectory in the joint space, and it can be expressed at the acceleration level as [see Eq. (2)]

$$\ddot{\mathbf{x}} = \mathbf{J} \ddot{\mathbf{q}} + \dot{\mathbf{J}} \dot{\mathbf{q}}$$

In the context of this work, the IK problem consists of the determination of $\dot{\mathbf{q}}$ according to a local optimization criterion in which the constraint of Eq. (2) is satisfied.

If an inertially referenced trajectory has to be tracked, \mathbf{J} represents the generalized Jacobian matrix [49] that, for a very massive spacecraft, approaches the Jacobian matrix of a fixed-based manipulator. On the other hand, if the manipulator has to track a trajectory defined with respect to a spacecraft-fixed reference frame, the manipulator Jacobian matrix has to be used [34].

If $k \leq 6$ is the dimension of the desired EE trajectory ($\mathbf{x}_d \in \mathbb{R}^k$) and n is the number of the DOF of the manipulator ($\mathbf{q} \in \mathbb{R}^n$), the degree of redundancy with respect to the EE task results in $r = n - k$. In the following, it is assumed $r \geq 1$; therefore, ∞^r solutions to the IK problem may exist. At each time step, the set of all possible solutions generates an r -dimensional subspace of the joint acceleration space. The general solution can be found by means of the Moore–Penrose generalized inverse of the Jacobian matrix:

$$\ddot{\mathbf{q}} = \mathbf{J}^+ (\ddot{\mathbf{x}}_d - \dot{\mathbf{J}} \dot{\mathbf{q}}) + \mathbf{Z} \ddot{\phi} \quad (11)$$

where $\mathbf{Z} = \mathbf{I} - \mathbf{J}^+ \mathbf{J}$.

If $r \geq d$, the problem of tracking a trajectory and in the meantime having null reaction components can be addressed [5,16,17], which can be formulated as

$$\text{find } \ddot{\mathbf{q}}: \begin{cases} \ddot{\mathbf{x}}(\ddot{\mathbf{q}}) = \ddot{\mathbf{x}}_d \\ {}^w\mathbf{R}(\ddot{\mathbf{q}}) = \mathbf{0} \end{cases} \quad (12)$$

[§]The inverse dynamics model that has been used in the simulated and experimental tests can be found in [48].

In particular, a unique solution is possible if $r = d$ (see Sec. IV.A), whereas if $r > d$, the number of possible solutions is ∞^{r-d} .

On the other hand, if $r < d$, the IK problem that leads to the local minimization of ${}^w\mathbf{R}$ can be formulated as

$$\text{find } \ddot{\mathbf{q}}: \begin{cases} \ddot{\mathbf{x}}(\ddot{\mathbf{q}}) = \ddot{\mathbf{x}}_d \\ {}^w\mathbf{R}(\ddot{\mathbf{q}}) \cong \mathbf{0} \end{cases} \quad (13)$$

The notation ${}^w\mathbf{R}(\ddot{\mathbf{q}}) \cong \mathbf{0}$ expresses the approximation to zero of ${}^w\mathbf{R}$ in a LS sense, according to [42], which is equivalent to the minimization of the cost function $f_R = \|{}^w\mathbf{R}(\ddot{\mathbf{q}})\|^2$.

In the solution to the local optimization problems of Eqs. (12) and (13), the linearity of $\ddot{\mathbf{x}}$ and ${}^w\mathbf{R}$ with respect to $\ddot{\mathbf{q}}$ will be used [see Eqs. (2) and (10)], since \mathbf{q} and $\dot{\mathbf{q}}$ can be considered as state variables.

Thanks to the structural similarity of the kinematics and dynamics equations for free-flying and fixed-based manipulators [34], the IK solutions presented in Sec. IV are applicable to both configurations. The simulation study and the experimental tests presented in Sec. VI have been carried out for a redundant three-DOF planar manipulator, fixed to the ground by means of a dynamometer in order to measure the reactions and experimentally validate the presented IK solutions.

IV. Inverse Kinematics Solutions

A. Extended Task-Space Solution

In the case of a nonredundant manipulator, which is in a non-singular configuration, the FK equation expressed at the acceleration level [Eq. (2)] can be directly inverted, resulting in the expression

$$\ddot{\mathbf{q}} = \mathbf{J}^{-1}(\ddot{\mathbf{x}}_d - \dot{\mathbf{J}}\dot{\mathbf{q}}) \quad (14)$$

On the other hand, in the case of a redundant manipulator in which $r = d$, the null reaction IK problem can be expressed as

$$\begin{cases} \mathbf{J}\ddot{\mathbf{q}} + \dot{\mathbf{J}}\dot{\mathbf{q}} = \ddot{\mathbf{x}}_d \\ \mathbf{M}\ddot{\mathbf{q}} + \mathbf{n} = \mathbf{0} \end{cases} \quad (15)$$

This problem, for each time step, can be regarded as a linear algebraic system in the $\ddot{\mathbf{q}}$ unknown, and its solution, if it exists, can be expressed as

$$\ddot{\mathbf{q}} = \begin{bmatrix} \mathbf{J} \\ \mathbf{M} \end{bmatrix}^{-1} \begin{bmatrix} \ddot{\mathbf{x}}_d - \dot{\mathbf{J}}\dot{\mathbf{q}} \\ -\mathbf{n} \end{bmatrix} \quad (16)$$

The matrix

$$\begin{bmatrix} \mathbf{J} \\ \mathbf{M} \end{bmatrix}$$

can be regarded as an extended Jacobian matrix [26,27], and the solution to the problem exists if and only if this matrix is square (which happens for $r = d$) and has full rank. This solution can be interpreted as an extension of the solution of Eq. (14), where the extended Jacobian matrix has the same role as the Jacobian matrix for the nonredundant manipulator.

B. Pseudoinverse of the Extended Jacobian Matrix Solution

In this section, the problem of minimizing the dynamic disturbances when the degree of redundancy of the manipulator is not sufficient to obtain a null ${}^w\mathbf{R}$ (i.e., when $r < d$) is addressed. In analogy with the solution based on the inverse of the Jacobian matrix for a nonredundant manipulator [Eq. (14)], if a redundant manipulator is considered, the LS solution to the IK problem, also known as pseudoinverse solution, can be expressed as

$$\ddot{\mathbf{q}} = \mathbf{J}^+(\ddot{\mathbf{x}}_d - \dot{\mathbf{J}}\dot{\mathbf{q}}) \quad (17)$$

which gives the minimum accelerations solution; that is, it provides the solution to the problem:

$$\begin{cases} \ddot{\mathbf{x}}(\ddot{\mathbf{q}}) = \ddot{\mathbf{x}}_d \\ \ddot{\mathbf{q}} \cong \mathbf{0} \end{cases} \quad (18)$$

The ETS approach of the previous section can be extended to the case of $r < d$ by means of a pseudoinversion, resulting in the expression

$$\ddot{\mathbf{q}} = \begin{bmatrix} \mathbf{J} \\ \mathbf{M} \end{bmatrix}^+ \begin{bmatrix} \ddot{\mathbf{x}}_d - \dot{\mathbf{J}}\dot{\mathbf{q}} \\ -\mathbf{n} \end{bmatrix} \quad (19)$$

which is the solution to the problem

$$\begin{bmatrix} \ddot{\mathbf{e}}(\ddot{\mathbf{q}}) \\ {}^w\mathbf{R}(\ddot{\mathbf{q}}) \end{bmatrix} \cong \mathbf{0} \quad (20)$$

where $\ddot{\mathbf{e}}(\ddot{\mathbf{q}}) \triangleq \ddot{\mathbf{x}}(\ddot{\mathbf{q}}) - \ddot{\mathbf{x}}_d$. The related cost function, which takes into account both $\ddot{\mathbf{e}}$ and ${}^w\mathbf{R}$, in this case is defined as

$$f_{x,R} \triangleq \|\ddot{\mathbf{e}}(\ddot{\mathbf{q}})\|^2 + \|{}^w\mathbf{R}(\ddot{\mathbf{q}})\|^2 \quad (21)$$

To define the relative importance between $\ddot{\mathbf{e}}$ and ${}^w\mathbf{R}$, two positive weighting coefficients λ_x and λ_R are introduced, resulting in the enhanced problem

$$\begin{bmatrix} \lambda_x \ddot{\mathbf{e}}(\ddot{\mathbf{q}}) \\ \lambda_R {}^w\mathbf{R}(\ddot{\mathbf{q}}) \end{bmatrix} \cong \mathbf{0} \quad (22)$$

The cost function of this problem is defined as

$$f_\lambda \triangleq \lambda_x^2 \|\ddot{\mathbf{e}}(\ddot{\mathbf{q}})\|^2 + \lambda_R^2 \|{}^w\mathbf{R}(\ddot{\mathbf{q}})\|^2 \quad (23)$$

and the related solution can be expressed as

$$\ddot{\mathbf{q}} = \begin{bmatrix} \lambda_x \mathbf{J} \\ \lambda_R \mathbf{M} \end{bmatrix}^+ \begin{bmatrix} \lambda_x (\ddot{\mathbf{x}}_d - \dot{\mathbf{J}}\dot{\mathbf{q}}) \\ -\lambda_R \mathbf{n} \end{bmatrix} \quad (24)$$

As an example, a parametric study on the reduction of the peak value of $\|{}^w\mathbf{R}\|$ that can be obtained when an increasing EE tracking error is accepted (i.e., when the ratio λ_x/λ_R is gradually decreased) is presented in Fig. 1. This simulation study has been carried out for the redundant three-DOF planar manipulator described in Sec. V in the hypothesis of rigid joints. The EE linear path presented in Fig. 2 and the weights $w_{Fx} = 0.05 \text{ N}^{-1}$, $w_{Fy} = 0.30 \text{ N}^{-1}$, and $w_T = 0.65 \text{ (N \cdot m)}^{-1}$ have been used.

It can be noticed that, as long as the ratio λ_x/λ_R is decreased, the position error of the EE becomes higher (i.e., the tip deviates from the desired trajectory, as illustrated in Fig. 2), while $\|{}^w\mathbf{R}\| \rightarrow 0$.

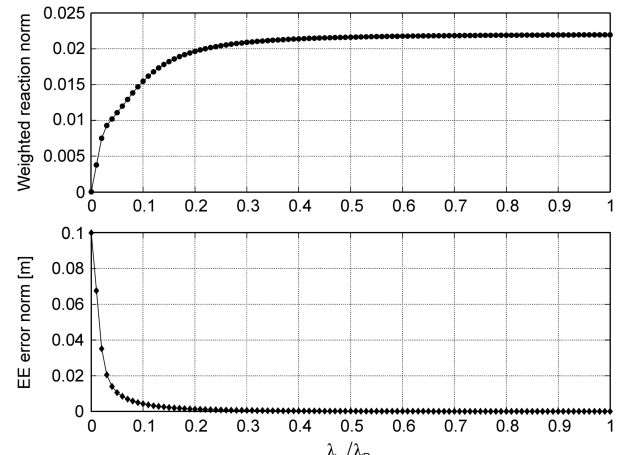


Fig. 1 Peak value of the weighted reaction norm and EE position error for different λ_x/λ_R ratios.

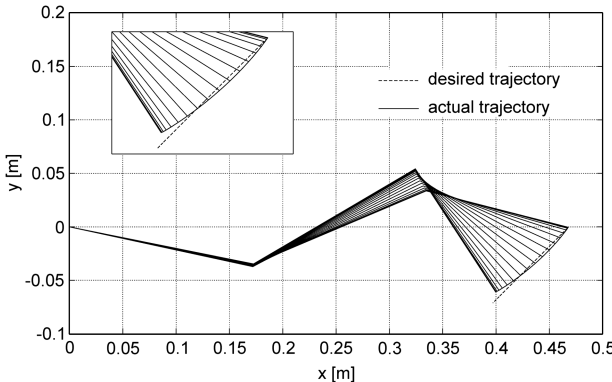


Fig. 2 Desired and actual EE trajectory ($\lambda_x/\lambda_R = 0.05$).

C. Least-Squares Solution with Equality Constraints

In this section, the weighted solution developed in the previous section [Eq. (24)] is used to derive the locally optimal solution that makes the manipulator track the EE trajectory and in the meantime minimize $\|{}^w R\|$. This optimization problem, defined in Eq. (13), can be expressed, making the dependence on \ddot{q} explicit, as

$$\begin{cases} \mathbf{J}\ddot{q} + \dot{\mathbf{J}}\dot{q} = \ddot{x}_d \\ M\ddot{q} + n \cong 0 \end{cases} \quad (25)$$

It can be noticed that Eq. (25) identifies a LSE problem in the \ddot{q} unknown. The FK equation defines the equality constraint. Among all the possible solutions to this constraint equation, the one of minimum $\|{}^w R\|$ has to be determined.

The solution to the LSE problem can be obtained, using the ETS approach, from Eq. (24) for $\lambda_x/\lambda_R \rightarrow \infty$, i.e., for $\ddot{e} \rightarrow 0$. The solution can be therefore expressed as

$$\ddot{q} = \lim_{\lambda_x/\lambda_R \rightarrow \infty} \left[\begin{array}{c} \lambda_x \mathbf{J} \\ \lambda_R M \end{array} \right]^{+} \left[\begin{array}{c} \lambda_x (\ddot{x}_d - \dot{\mathbf{J}}\dot{q}) \\ -\lambda_R n \end{array} \right] \quad (26)$$

This formulation of the solution is equivalent to the weighting method [42–44], where the weight $\mu = \lambda_x/\lambda_R$ has to be used.

It should be noticed that a formal similarity exists between the solution for the null reaction [Eq. (16)] and for the minimum reaction problem [Eqs. (19), (24), and (26)], in which the role of the inverse of the extended Jacobian matrix in the first case is played by the pseudoinverse of the extended Jacobian matrix in the second case. In addition, a value of $\mu = \lambda_x/\lambda_R \rightarrow \infty$ has to be used in Eq. (24) if a zero EE tracking error is required.

A finite value of μ has to be used in the numerical implementation, and criteria for its consistent choice, together with efficient and stable numerical methods for the solution, have been presented in literature [42–44]. Furthermore, it has been noticed [42,44] that if a LS routine is available on the onboard computer, no further implementation is needed in order to obtain the LSE solution through this approach.

A closed-form solution can also be found for the LSE problem [Eq. (25)] by using the pseudoinverse of the Jacobian matrix [42]. First, the value of $\ddot{\phi}$ in Eq. (11) has to be determined. If the \ddot{q} solution of Eq. (11) is substituted in the inverse dynamics equation of ${}^w R$ [Eq. (10)], the following expression can be obtained:

$${}^w R(\ddot{\phi}) = [M Z] \ddot{\phi} + M J^+ (\ddot{x}_d - \dot{\mathbf{J}}\dot{q}) + n \quad (27)$$

The solution that provides the minimum base reaction is

$$\ddot{\phi} = [M Z]^+ [-M J^+ (\ddot{x}_d - \dot{\mathbf{J}}\dot{q}) - n] \quad (28)$$

Finally, substituting $\ddot{\phi}$ in Eq. (11), and using the property $Z[M Z]^+ = [M Z]^+$, the closed-form solution to the LSE problem is obtained:

$$\ddot{q} = J^+ (\ddot{x}_d - \dot{\mathbf{J}}\dot{q}) - [M Z]^+ [M J^+ (\ddot{x}_d - \dot{\mathbf{J}}\dot{q}) + n] \quad (29)$$

The LSE solution presented in this section, and its extension that takes into account the joint acceleration limits presented in the following section, results are suitable for real-time implementation by means of a two-step solution. First, efficient recursive formulations [50,51] have to be used in order to numerically compute the needed kinematic and dynamic variables (J , $\dot{J}\dot{q}$, M , and n). Then, Eq. (25) can be solved in real time by means of recursive algorithms [35], by means of solution techniques used for the more general constrained quadratic programming problem [36–39], or by means of neural networks algorithms [40,41].

Concerning the reliability of the solution, robust recursive methods exist [35], which assure that the kinematic constraint is always satisfied, even in presence of numerical errors. Moreover, feedback techniques [20] can be profitably used in the sensory data-driven control in case of using new fast algorithms with poor numerical properties.

D. Least-Squares Solution with Equality and Inequality Constraints

A useful extension of the LSE problem [Eq. (25)] can be made by introducing joint acceleration limits to the solution, which ensure that the manipulator is working inside the physical acceleration and torque limits of its joints and motors. Moreover, the introduction of joint acceleration limits may help in the control of the maximum joint velocities and positions [41,52], and it represents an indirect method to avoid the algorithmic singularities that may occur when local optimization methods are used [53,54].

The LS problem with equality and inequality constraints (LSEI) can be formulated as [42]

$$\begin{cases} \mathbf{J}\ddot{q} + \dot{\mathbf{J}}\dot{q} = \ddot{x}_d \\ M\ddot{q} + n \cong 0 \\ \ddot{q}_l \leq \ddot{q} \leq \ddot{q}_u \end{cases} \quad (30)$$

The inequalities are interpreted componentwise, and the acceleration limits may in general be different for each joint.

It has to be noticed that the presence of inequality constraints makes it not possible to obtain a closed-form solution in this case. Nevertheless, the algorithms used for the real-time solution of the LSE problem have been developed (or modified) in order to be suitable also for the solution of the LSEI problem [35–41].

If the imposed acceleration limits are too low with respect to the desired EE motion law, more acceleration limits may become active, thus reducing the effective degree of redundancy $r_{\text{eff}} = r - n_{\text{lim}}$. If $r_{\text{eff}} = 0$, no optimization can be performed, and a local peak of $\|{}^w R\|$ is generated. A remedy method is to use time-scaled EE trajectories in these cases. For example, if $r = 1$, when one acceleration limit is active, the redundancy is lost and no optimization can be performed, causing an increase of the peak value of $\|{}^w R\|$. Moreover, for a determined manipulator geometry and EE trajectory, the minimization performance is lower (i.e., the peak value of $\|{}^w R\|$ is higher), as long as the absolute values of the acceleration limits are decreased.

As an example, the increase of the peak reaction due to decreasing acceleration limits and the related joint accelerations are presented in Fig. 3. The simulations have been carried out for the same robot model, EE trajectory, and weights in ${}^w R$ as in the rigid joints simulations of Sec. VI.A.

V. Experimental Setup

The experimental setup is designed in order to experimentally validate the IK solutions presented in Sec. IV. The robotic arm is suspended using an air-bearings system, and it is fixed to the ground by means of a custom design dynamometer in order to measure the forces and torques transferred to the ground during its maneuvers [55,56]. The experimental setup, which is composed of the robotic

arm system, the air-bearings suspension system, and the measurement system, is shown in Fig. 4.

A. Robotic Arm System

The robotic arm used in this study was previously designed to perform experiments on ESA parabolic flights [55,57–59]; therefore, it can operate in zero gravity in a three-dimensional workspace. The robot links have a modular and symmetrical design: this allows the increasing or decreasing of the number of links and the modification of the orientation of the joint rotation axes. In particular, in the two-dimensional setup used in this study, a three-link configuration is used ($n = 3$) in which the joint axes are parallel to each other.

The manipulator is driven by DC servomotors with velocity command input. A decentralized proportional-integral-derivative (PID)-type control is used, which is implemented on a Robox RMC4 motion controller.

The robot joints cannot be considered infinitely rigid, mainly because of the flexibility of the motor reduction gear and of the joint transmission, as it happens in the majority of space robotics applications. On the other hand, the robot links can be considered rigid with good approximation, as they are based on a rigid cylindrical composite structure (see Fig. 4).

The arm inertial parameters and the stiffness and damping characteristics of the joints and of the dynamometer were experimentally determined [60]. The main geometrical and inertial properties of the robotic arm are presented in Table 1.

The rotational stiffness curve of the first joint, and the plot of the step response test used for the measure of ζ , are presented for illustrative purposes in Figs. 5 and 6.

The values $\zeta = 1.041 \cdot 10^{-2}$ and $f_n = 1.16$ Hz were calculated from the experimental data [60].

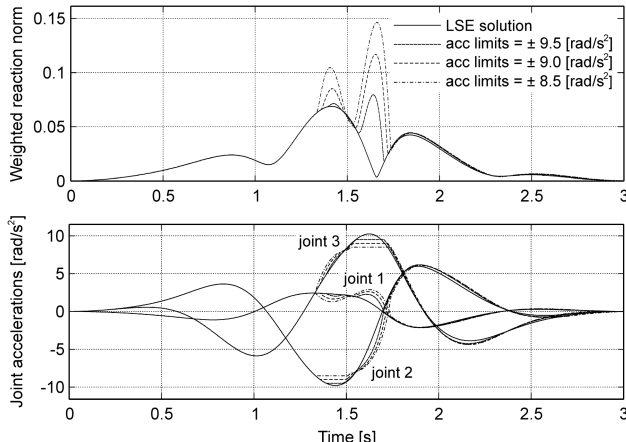


Fig. 3 Increase of the peak reaction due to the introduction of joint acceleration limits.



Fig. 4 Experimental setup.

Table 1 Robot main geometrical and inertial properties

	Link 1	Link 2	Link 3
l , m	0.176	0.176	0.135
l_G , m	0.115	0.115	0.056
m , kg	0.615	0.615	0.200
I_{Gx} , kgm ²	$2.43 \cdot 10^{-4}$	$2.43 \cdot 10^{-4}$	$1.21 \cdot 10^{-4}$
I_{Gy} , kgm ²	$2.73 \cdot 10^{-3}$	$2.73 \cdot 10^{-3}$	$1.24 \cdot 10^{-3}$
I_{Gz} , kgm ²	$2.73 \cdot 10^{-3}$	$2.73 \cdot 10^{-3}$	$1.24 \cdot 10^{-3}$

B. Suspension System

The suspension system is based on air bearings, which work on a granite plane [55,56]. This system is used in order to compensate for the weight of the robot links and prevent their deflection due to the gravity force. The air bearings are positioned under each robot joint, as shown in Fig. 4.

C. Measurement System

The first robot joint is connected to the dynamometer through a rigid flange. The dynamometer is made of two polymeric beams having a square cross section [55,56]. A polymeric material has been used in order to enhance the measurement system sensitivity thanks to its small Young modulus. The forces in the two planar directions and the torque around the axis perpendicular to the granite plane are measured by transducing the deformation of the polymeric beams with strain gauges: two full Wheatstone bridges are used for each beam, one for each planar direction.

The measurement system is presented in Fig. 7, and the dynamometer main specifications are summarized in Table 2.

VI. Simulation and Experimental Results

The IK solutions presented in Sec. IV are implemented on a MATLAB simulator in order to test their performance for the planar robot described in the previous section in the hypothesis of rigid joints. The simulator is composed of two main modules: the first module solves the IK problem according to the desired scheme

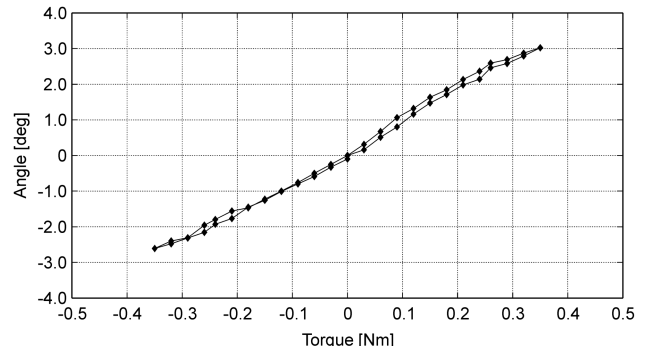


Fig. 5 Joint rotational stiffness curve.

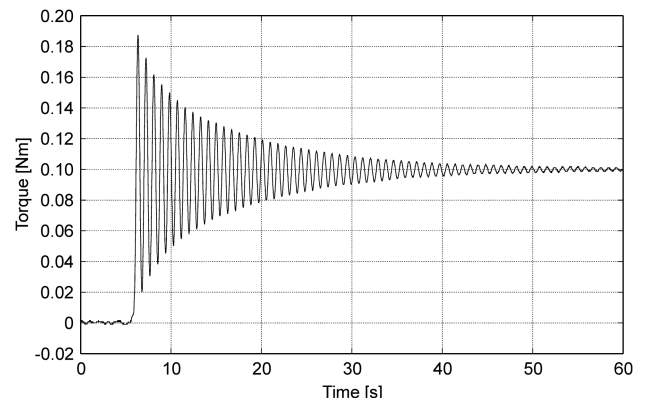


Fig. 6 Joint step response.

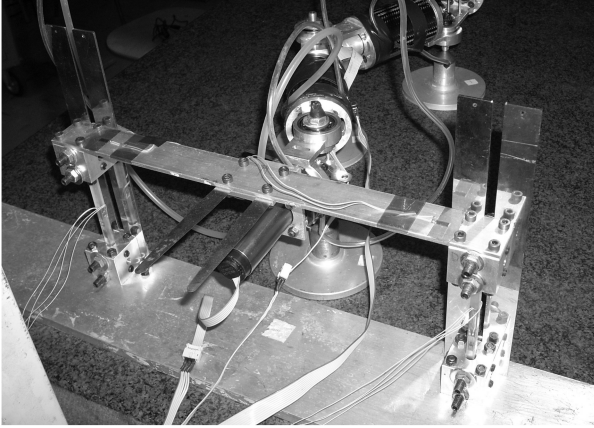


Fig. 7 Measurement system.

(LS, LSE, or LSEI), and the second one then solves the inverse dynamics using the joint accelerations generated by the first module.

The desired EE trajectory has dimension $k = 2$ (x and y coordinates), since only the position and not the orientation of the EE is controlled. Therefore, $r = n - k = 1$.

Two test cases are considered: in the first test case, the minimization of $\|{}^w \mathbf{R}\|$, which comprises both torque and forces, is considered, whereas in the second test case, the planar torque transferred to the ground T_{Bz} has to be minimized. A circular EE trajectory of diameter $D = 0.1$ m is used in both test cases. The initial configuration of the arm (joint relative coordinates) is

$$\mathbf{q}(t_0) = [-0.20 \quad 0.60 \quad -0.65]^T \text{ rad} \quad (31)$$

Simulations are used in order to compare $\|{}^w \mathbf{R}\|$, or T_{Bz} , for the given EE trajectory in the case of using the LS, the LSE, or the LSEI solution. In the third case, a joint acceleration constraint of 8.73 rad/s^2 is imposed. In particular, the peak reactions resulting from the LSE and LSEI solutions are compared with those resulting from the classical LS one, which is taken as a reference in order to evaluate their performance.

The same EE trajectory and the related joint accelerations derived from the three IK solutions (LS, LSE, and LSEI) are used to perform the experimental tests for their validation. Moreover, the experimental tests allowed to evaluate how the performance predicted by the rigid joints simulator can be modified when implemented in a real system in which joint flexibility cannot be neglected.

To have a better understanding of the effect of joint flexibility, a multibody model of the experimental robot that takes into account the joint and the dynamometer stiffness and damping is also used. The flexible joints multibody simulator, developed by means of the MD Adams software, was already validated as presented in [60].

A. Weighted Reaction Minimization

The first test case is related to the minimization of $\|{}^w \mathbf{R}\|$, therefore involving both the reaction torque T_{Bz} and the reaction forces F_{Bx} and F_{By} , according to the definition of Eq. (5) explicitated for the planar case. In this case, ${}^w \mathbf{R}$ is composed of three independent components; therefore, it is not possible to obtain a null value for

Table 2 Dynamometer main specifications

Parameter	Value
Maximum force in x and y directions	1 N
Resolution (force)	$1.7 \cdot 10^{-3}$ N
Accuracy (force)	$\pm 5.4 \cdot 10^{-2}$ N
Maximum torque around z axis	$0.320 \text{ N} \cdot \text{m}$
Resolution (torque)	$2.6 \cdot 10^{-4} \text{ N} \cdot \text{m}$
Accuracy (torque)	$\pm 8.5 \cdot 10^{-3} \text{ N} \cdot \text{m}$
First eigenfrequency (robot and dynamometer)	>15 Hz

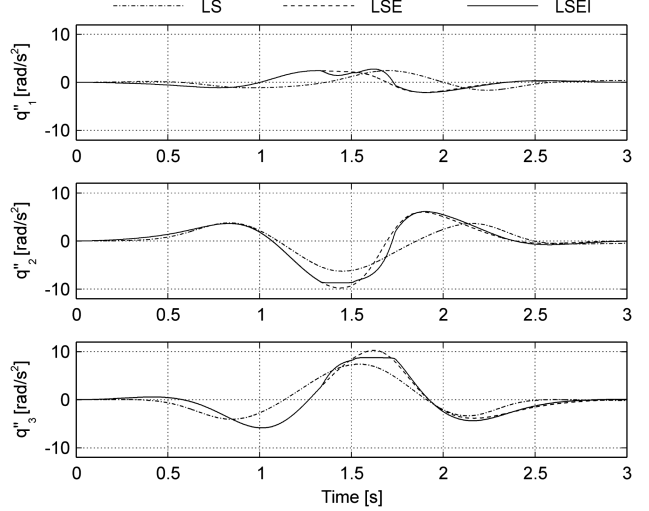


Fig. 8 Joint acceleration profiles in the weighted reaction minimization test case (LS, LSE, and LSEI).

its norm during the trajectory execution by exploiting 1 deg of redundancy only.

In the simulations, the weights $w_{Fx} = 0.05 \text{ N}^{-1}$, $w_{Fy} = 0.30 \text{ N}^{-1}$, and $w_T = 0.65 \text{ (N} \cdot \text{m})^{-1}$ are used.

The joint accelerations and the stroboscopic views of the robot motion for the three considered cases (LS, LSE, and LSEI) are presented in Figs. 8 and 9.

In Fig. 10, the LS, LSE, and LSEI profiles of $\|{}^w \mathbf{R}\|$ are overlapped in order to show the reaction reduction capability of the LSE and LSEI solutions with respect to the LS one, which is taken as a reference, in the ideal case (rigid joints), in the simulations with flexible joints, and in the experimental tests. A summary of the performances obtained in this and in the following test case will be presented in Sec. VI.C (see Table 3).

The following discussion is aimed at studying the effect of joint flexibility on the difference, in terms of the reaction transferred to

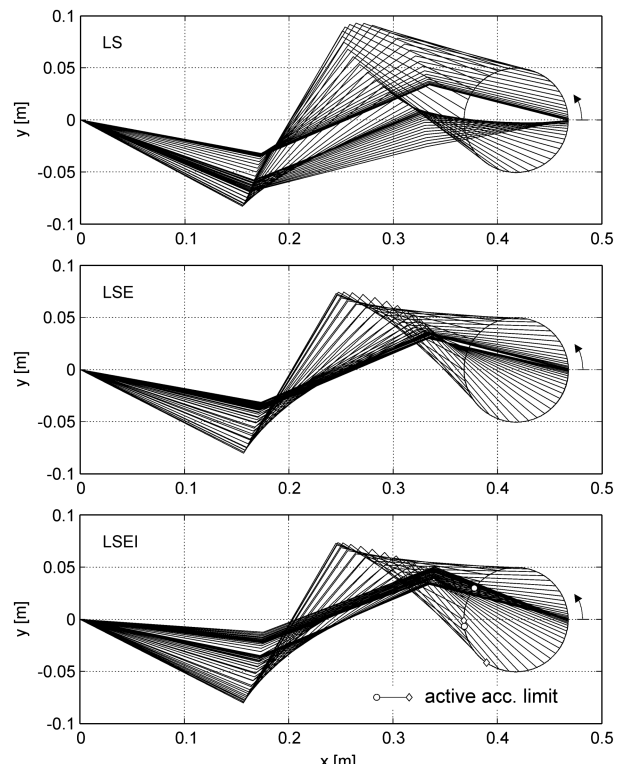


Fig. 9 Stroboscopic views of the robot motion in the weighted reaction minimization test case (LS, LSE, and LSEI).

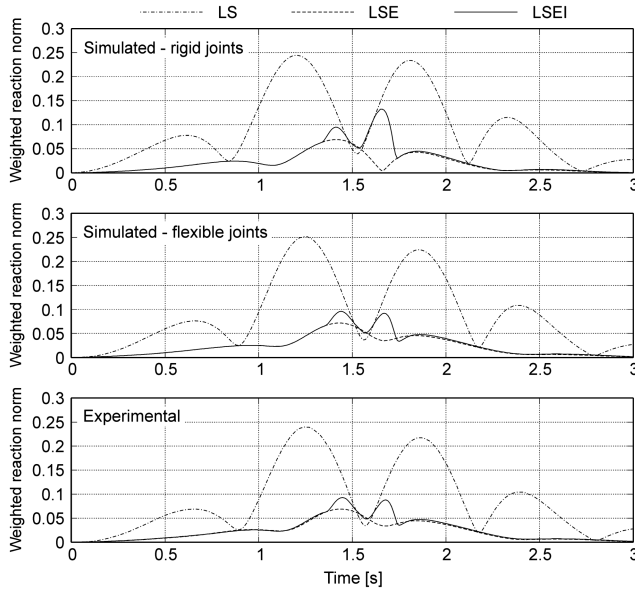


Fig. 10 Comparison of the LS, LSE, and LSEI weighted reaction norm in the simulation and experimental tests.

the ground, between the ideal rigid joints simulations and the experimental tests.

The total reaction error δ_{tot} is defined as the instantaneous difference between the value of the weighted reaction norm computed in the simulations with rigid joints ($\|{}^w \mathbf{R}_\infty\|$) and the same variable measured in the experimental tests ($\|{}^w \mathbf{R}_{\text{exp}}\|$) as expressed in Eq. (34). In addition, δ_{tot} can be divided in two components, δ_{flex} and δ_{mod} :

$$\delta_{\text{flex}} \triangleq \|{}^w \mathbf{R}_\infty\| - \|{}^w \mathbf{R}_k\| \quad (32)$$

$$\delta_{\text{mod}} \triangleq \|{}^w \mathbf{R}_k\| - \|{}^w \mathbf{R}_{\text{exp}}\| \quad (33)$$

$$\delta_{\text{tot}} = \delta_{\text{flex}} + \delta_{\text{mod}} \triangleq \|{}^w \mathbf{R}_\infty\| - \|{}^w \mathbf{R}_{\text{exp}}\| \quad (34)$$

where $\|{}^w \mathbf{R}_k\|$ is the weighted reaction norm computed in the simulations performed with the flexible joints simulator. The total reaction error δ_{tot} is composed of a term that depends on the joint flexibility (i.e., on the joint stiffness and damping), and therefore can be modeled (δ_{flex}), and a term (δ_{mod}) that comprises the uncertainty on the dynamic parameters used in the flexible joints multibody simulator [60] (i.e., the arm inertial parameters and the joint and dynamometer stiffness and damping) and all the other not modeled effects, such as the joint and the dynamometer hysteresis, the joint backlash, the uncertainty of the control system, and the effect of harness and of the pressurized air cables.

The total reaction error δ_{tot} and its components δ_{flex} and δ_{mod} are overlapped in Fig. 11 for the LS, LSE, and LSEI solutions.

In Fig. 12, a parametric study is presented on the influence of the robotic arm mass and the payload mass on $\|{}^w \mathbf{R}\|$ in the LS and LSE cases. The mass ratio is similarly defined as $k_m = (m_a/m_A) \cdot 100 [\%]$ in the case of the arm mass (the moments of inertia of the robot links are varied proportionally) and $k_m = (m_p/m_A) \cdot 100 [\%]$ in the case of

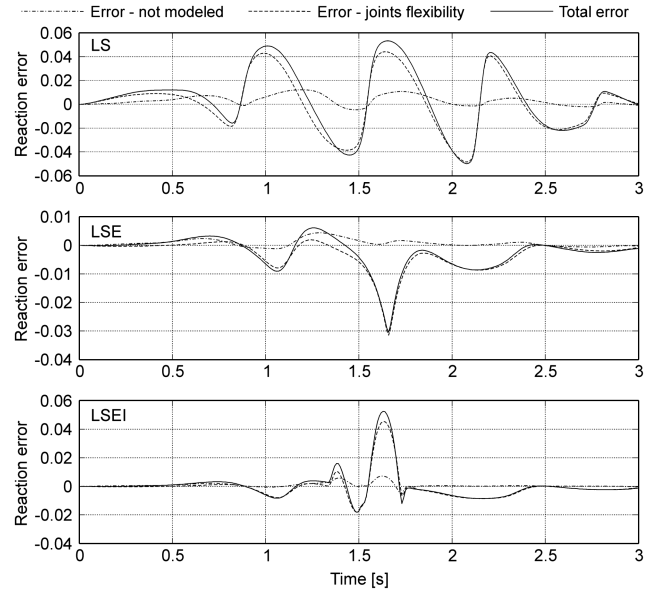


Fig. 11 Total reaction error and its components (LS, LSE, and LSEI).

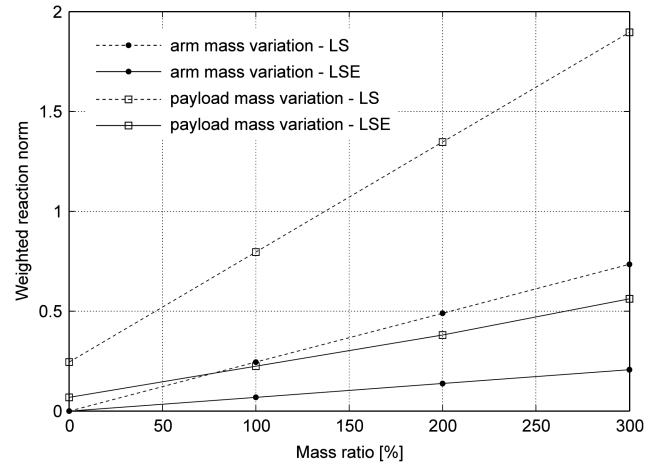


Fig. 12 Peak weighted reaction norm for increasing arm mass and payload mass.

the payload mass. The EE trajectory and the reaction weights used in this study are the same as previously used in this section.

From the analysis of Fig. 12, it can be noticed that, in all the considered cases, the LS reaction is higher than the LSE one and that the slope of the LS curve is higher than the LSE one, both in case of varying m_a and m_p . Moreover, the slope of the curve related to the variation of m_p is higher than the one related to the variation of m_a , both in the LS and in the LSE cases. This is due to the fact that higher reactions are expected if m_p is increased with respect to the case of a uniform arm mass increase.

B. Reaction Torque Minimization

The second test case is related to the minimization of T_{Bz} . In this case, $r = d$; therefore, the feasibility of an exactly null reaction torque can be studied.

The stroboscopic views of the robot motion for the three considered cases (LS, LSE, and LSEI) are presented in Fig. 13.

In Fig. 14, the LS, LSE, and LSEI profiles of $\|T_{Bz}\|$ are overlapped in order to show the torque reduction capability of the LSE and LSEI solutions with respect to the LS one in the ideal case (rigid joints), in the simulations with flexible joints, and in the experimental tests.

From the comparison of Figs. 10 and 14, it can be noticed that in the first case, the presence of 1 deg of redundancy is not sufficient to obtain a null reaction, whereas this is possible in the second case.

Table 3 Performance indicator for the LSE and LSEI solutions in the simulation and experimental tests

	Weighted reaction minimization, %	Reaction torque minimization, %
LSE-rigid joints	72.0	100
LSE-flexible joints	71.7	90.9
LSE-experimental	71.4	90.8
LSEI-rigid joints	46.6	60.9
LSEI-flexible joints	61.9	63.7
LSEI-experimental	61.4	63.4

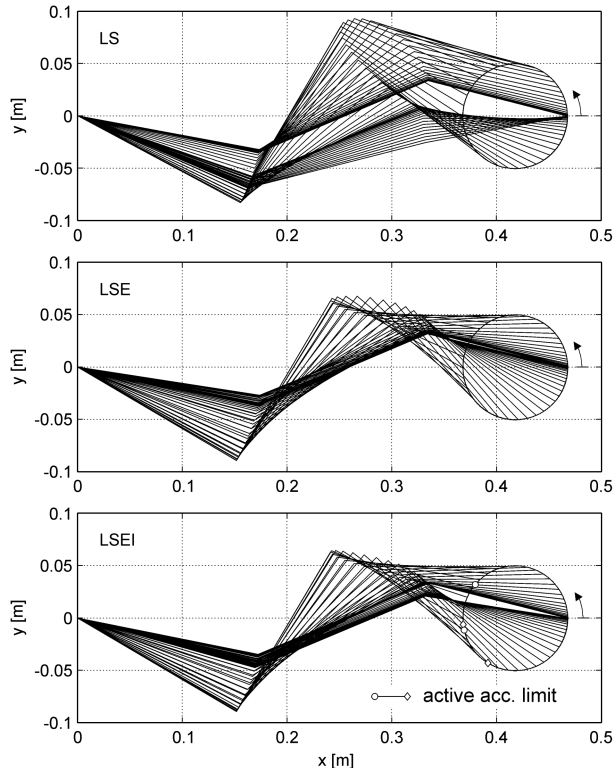


Fig. 13 Stroboscopic views of the robot motion in the reaction torque minimization test case (LS, LSE, and LSEI).

Moreover, in both cases, the LSE and LSEI reactions have the same profile up to the time in which the first joint acceleration limit becomes active. Then, when the acceleration limit is active, a local increase in the reactions can be observed in both cases.

C. Discussion on Simulation and Experimental Results

A performance indicator (PI) is defined for the evaluation of the performance of the minimization in the LSE and LSEI cases with respect to the LS one:

$$\text{PI} \triangleq 100 \cdot \left(1 - \frac{\|{}^w\mathbf{R}\|_{\text{IKS,max}}}{\|{}^w\mathbf{R}\|_{\text{LS,max}}} \right) \% \quad (38)$$

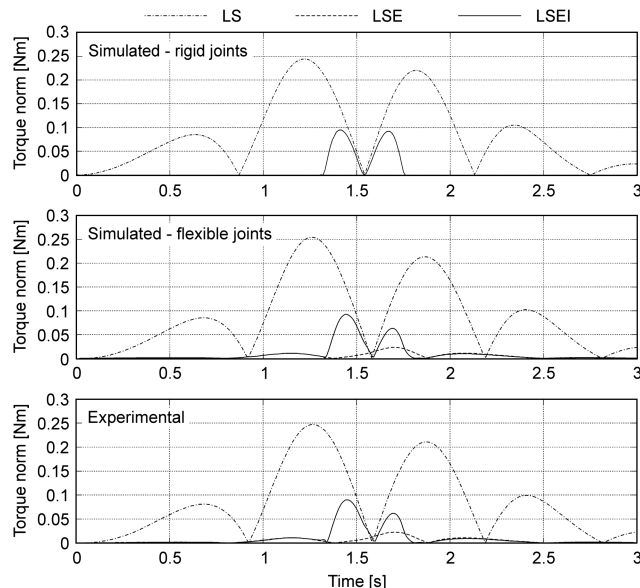


Fig. 14 Comparison of the LS, LSE, and LSEI torque norm in the simulation and experimental tests.

where IKS = LS, LSE, or LSEI represents the IK solution used, and the subscript max means that the peak value of the involved variable has to be considered.

A summary of the performance of the LSE and LSEI solutions in the minimization of $\|{}^w\mathbf{R}\|$ for the considered test cases is presented in Table 3. Note that, in the reaction torque minimization test case, $\|{}^w\mathbf{R}\| = \|T_{Bz}\|$.

In the weighted reaction minimization test case, the value of PI in the LSE-rigid joints case is 72.0%, whereas it is 71.4% in the experimental tests. On the other hand, in the LSEI-rigid joints case, PI = 46.6%, which raises up to 61.4% in the experimental tests. This is due to the fact that, in the LSEI case, the joint flexibility causes a reduction of the peak value of $\|{}^w\mathbf{R}\|$, resulting in a higher PI.

In the reaction torque minimization test case, PI = 100% for the LSE solution in the case of rigid joints; that is, in this case, it is possible to exploit the redundant degree of freedom for the realization of a null reaction torque. In the experimental tests, due to the joint flexibility, the performance indicator is reduced to PI = 90.8%.

On the other hand, in the LSEI-rigid joints case, PI = 60.9%, whereas in the experimental tests, PI = 63.4%. Similar to the first test case, the joint flexibility causes little reduction in the peak torque, resulting in a slightly higher PI.

Concerning the effect of joint flexibility, it has to be noticed that δ_{flex} is a very important component of δ_{tot} in all the considered cases: its norm ranges from 82.7% up to 103.3% of the norm of δ_{tot} (peak values). This effect could be limited by using slower EE trajectories or a robot with increased joint stiffness.

The proposed reaction minimization method therefore shows good performance in the reduction of $\|{}^w\mathbf{R}\|$ in the ideal case (rigid joints), with and without an active acceleration limit. Moreover, even if δ_{tot} is not negligible, a very similar performance is also obtained in the experimental tests.

As a drawback, in the LSE solution, the maximum joint accelerations increase 70% with respect to the LS ones in both test cases in order to perform the optimization.

A better performance is expected for higher-DOF manipulators, similar to what presented in [13]. In particular, if $r \geq d$, zero reaction paths can be studied [5]. Moreover, even though n_{lim} acceleration limits are active (which reduce the effective degree of redundancy $r_{\text{eff}} = r - n_{\text{lim}}$), if there are enough DOF such that $r_{\text{eff}} \geq 1$, the minimization algorithm is still effective in reducing reactions.

VII. Conclusions

In this paper, a novel solution for the IK of redundant space manipulators is presented, which is aimed at locally minimizing the dynamic disturbances transferred to the spacecraft. The solution, which is based on a CLS approach and is suitable for real-time implementation, is introduced in the context of a more general theory. In particular, the proposed solution has been derived both in the framework of the TP solution, in which a closed-form solution is given, and in the framework of the ETS solution, in which the use of increasing weights makes the ETS solution approach the TP one. From the implementation point of view, the solution can be computed in real time by using solution techniques for the LSE problem or by using the weighting method, which only needs simple LS routines. The weighting method has the additional advantages that it can be easily extended to multicriteria optimization and that the minimization performance can be enhanced by relaxing the EE tracking requirements.

In the LSEI solution, joint acceleration constraints are introduced in order to take into account the physical limits of the manipulator joints. When one, or more, acceleration limits are active, the degree of redundancy is accordingly reduced, and this may cause an increase of the peak reaction. An interesting characteristic of this solution is also that joint limits and joint velocity limits could be taken into account.

The proposed solutions have been tested by simulation and experimentally validated for a three-DOF manipulator, and they show good performance in the reduction of the dynamic disturbances, with and

without an active acceleration limit. In particular, it has been shown that a null reaction can be obtained if the number of redundant DOF is equal to the number of reaction components to be controlled. In the experimental tests, a limited reaction error due to the joint flexibility is present, which can be reduced by increasing joint stiffness or time-scaling the EE trajectory. A drawback of the proposed solutions, which is common to any other reaction minimization technique, is that significantly higher joint accelerations are needed with respect to the classical LS solution in order to perform the optimization task. The analysis of the performance and the implementation of the proposed solutions in three-dimensional and in higher-DOF applications will be part of future work.

Acknowledgment

The authors would like to thank Francesco Angrilli of the University of Padova for the financial support and for the helpful discussions and suggestions on the scientific topics of this work.

References

- [1] Dubowsky, S., and Papadopoulos, E., "The Kinematics, Dynamics, and Control of Free-Flying and Free-Floating Space Robotic Systems," *IEEE Transactions on Robotics and Automation*, Vol. 9, No. 5, 1993, pp. 531–543.
doi:10.1109/70.258046
- [2] Oda, M., "Attitude Control Experiments of a Robot Satellite," *Journal of Spacecraft and Rockets*, Vol. 37, No. 6, 2000, pp. 788–794.
doi:10.2514/2.3636
- [3] Yoshida, K., "Engineering Test Satellite VII Flight Experiments for Space Robot Dynamics and Control: Theories on Laboratory Test Beds Ten Years Ago, Now in Orbit," *The International Journal of Robotics Research*, Vol. 22, No. 5, 2003, pp. 321–335.
doi:10.1177/0278364903022005003
- [4] Miller, J. H., "The Dynamic Effects of Internal Robots on Space Station Freedom," AIAA Guidance, Navigation, and Control Conference, AIAA Paper 1991-2822, 1991.
- [5] Nenchev, D., Umetani, Y., and Yoshida, K., "Analysis of a Redundant Free-Flying Spacecraft/Manipulator System," *IEEE Transactions on Robotics and Automation*, Vol. 8, No. 1, 1992, pp. 1–6.
doi:10.1109/70.127234
- [6] Caccavale, F., and Siciliano, B., "Kinematic Control of Redundant Free-Floating Robotic Systems," *Advanced Robotics*, Vol. 15, No. 4, 2001, pp. 429–448.
doi:10.1163/156855301750398347
- [7] Nenchev, D., Yoshida, K., and Umetani, Y., "Analysis, Design and Control of Free-Flying Space Robots Using Fixed-Attitude-Restricted Jacobian Matrix," *Proceedings of the 5th International Symposium on Robotics Research*, edited by H. Miura, and S. Arimoto, MIT Press, Cambridge, MA, 1991, pp. 251–258.
- [8] Dubowsky, S., and Torres, M. A., "Path Planning for Space Manipulators to Minimize Spacecraft Attitude Disturbances," *Proceedings of the 1991 IEEE International Conference on Robotics and Automation*, Sacramento, CA, Vol. 3, IEEE Publ., Piscataway, NJ, 1991, pp. 2522–2528.
doi:10.1109/ROBOT.1991.132005
- [9] Torres, M. A., and Dubowsky, S., "Minimizing Spacecraft Attitude Disturbances in Space Manipulator Systems," *Journal of Guidance, Control, and Dynamics*, Vol. 15, No. 4, 1992, pp. 1010–1017.
doi:10.2514/3.20936
- [10] Nakamura, Y., and Mukherjee, R., "Nonholonomic Path Planning of Free-Flying Space Robots via a Bi-Directional Approach," *IEEE Transactions on Robotics and Automation*, Vol. 7, No. 4, 1991, pp. 500–514.
doi:10.1109/70.86080
- [11] Nakamura, Y., and Mukherjee, R., "Exploiting Nonholonomic Redundancy of Free-Flying Space Robots," *IEEE Transactions on Robotics and Automation*, Vol. 9, No. 4, 1993, pp. 499–506.
doi:10.1109/70.246062
- [12] De Silva, C. W., "Trajectory Design for Robotic Manipulators in Space Applications," *Journal of Guidance, Control, and Dynamics*, Vol. 14, No. 3, 1991, pp. 670–674.
doi:10.2514/3.20691
- [13] Quinn, R. D., Chen, L., and Lawrence, C., "Base Reaction Control for Space-Based Robots Operating in Microgravity Environment," *Journal of Guidance, Control, and Dynamics*, Vol. 17, No. 2, 1994, pp. 263–270.
- [14] Shäfer, B., Krenn, R., and Rebele, B., "On Inverse Kinematics and Kinetics of Redundant Space Manipulator Simulation," *Journal of Computational and Applied Mechanics*, Vol. 4, No. 1, 2003, pp. 53–70.
- [15] Krenn, R., and Hirzinger, G., "Modular, Generic Inverse Kinematics Algorithm Applied to Kinematically Redundant Space Manipulators," 8th ESA Workshop on Advanced Space Technologies for Robotics and Automation, ESA WPP-236, ESA Publications Division, Noordwijk, The Netherlands, 2004.
- [16] Nenchev, D. N., Yoshida, K., and Vichitkulsawat, P., "Reaction Null-Space Control of Flexible Structure Mounted Manipulator Systems," *IEEE Transactions on Robotics and Automation*, Vol. 15, No. 6, 1999, pp. 1011–1023.
doi:10.1109/70.817666
- [17] Yoshida, K., Nenchev, D. N., and Uchiyama, M., "Moving Base Robotics and Reaction Management Control," *Proceedings of the 7th International Symposium on Robotics Research*, edited by G. Giralt, and G. Hirzinger, Springer–Verlag, Berlin, 1996, pp. 101–109.
- [18] Cocuzza, S., Pretto, I., Menon, C., and Angrilli, F., "Control of Dynamic Attitude Disturbances on Spacecrafts Equipped with Robotic Systems for Orbital Maintenance," 58th International Astronautical Congress, Hyderabad, India, International Astronautical Federation Paper IAC-07-C1.8.01, 2007.
- [19] Whitney, D. E., "Resolved Motion Rate Control of Manipulators and Human Prostheses," *IEEE Transactions on Man-Machine Systems*, Vol. 10, No. 2, 1969, pp. 47–53.
doi:10.1109/TMMS.1969.299896
- [20] Luh, J. Y. S., Walker, M. W., and Paul, R. P. C., "Resolved-Acceleration Control of Mechanical Manipulators," *IEEE Transactions on Automatic Control*, Vol. 25, No. 3, 1980, pp. 468–474.
doi:10.1109/TAC.1980.1102367
- [21] Nenchev, D. N., "Redundancy Resolution through Local Optimization: A Review," *Journal of Robotic Systems*, Vol. 6, No. 6, 1989, pp. 769–798.
doi:10.1002/rob.4620060607
- [22] Siciliano, B., "Kinematic Control of Redundant Robot Manipulators: A Tutorial," *Journal of Intelligent and Robotic Systems: Theory and Applications*, Vol. 3, No. 3, 1990, pp. 201–212.
doi:10.1007/BF00126069
- [23] Klein, C. A., and Huang, C. H., "Review of Pseudoinverse Control for Use with Kinematically Redundant Manipulators," *IEEE Transactions on Systems, Man, and Cybernetics*, Vol. 13, No. 3, 1983, pp. 245–250.
- [24] Wampler, C. W., "Manipulator Inverse Kinematic Solutions Based on Vector Formulations and Damped Least-Squares Methods," *IEEE Transactions on Systems, Man, and Cybernetics*, Vol. 16, No. 1, 1986, pp. 93–101.
doi:10.1109/TSMC.1986.289285
- [25] Liégeois, A., "Automatic Supervisory Control of the Configuration and Behavior of Multibody Mechanisms," *IEEE Transactions on Systems, Man, and Cybernetics*, Vol. 7, No. 12, 1977, pp. 868–871.
doi:10.1109/TSMC.1977.4309644
- [26] Oh, S. Y., Orin, D., and Bach, M., "An Inverse Kinematic Solution for Kinematically Redundant Robot Manipulators," *Journal of Robotic Systems*, Vol. 1, No. 3, 1984, pp. 235–249.
doi:10.1002/rob.4620010303
- [27] Baillieul, J., "Kinematic Programming Alternatives for Redundant Manipulators," *Proceedings of the 1985 IEEE International Conference on Robotics and Automation*, Vol. 2, IEEE Computer Society Press, Silver Spring, MD, 1985, pp. 722–728.
- [28] Nakamura, Y., Hanafusa, H., and Yoshikawa, T., "Task-Priority Based Redundancy Control of Robot Manipulators," *The International Journal of Robotics Research*, Vol. 6, No. 2, 1987, pp. 3–15.
doi:10.1177/027836498700600201
- [29] Maciejewski, A. A., and Klein, C. A., "Obstacle Avoidance for Kinematically Redundant Manipulators in Dynamically Varying Environments," *The International Journal of Robotics Research*, Vol. 4, No. 3, 1985, pp. 109–117.
doi:10.1177/027836498500400308
- [30] Hollerbach, J. M., and Suh, K. C., "Redundancy Resolution of Manipulators through Torque Optimization," *IEEE Journal of Robotics and Automation*, Vol. 3, No. 4, 1987, pp. 308–316.
doi:10.1109/JRA.1987.1087111
- [31] Vukobratovic, M., and Kircanski, M., "A Dynamic Approach to Nominal Trajectory Synthesis for Redundant Manipulators," *IEEE Transactions on Systems, Man, and Cybernetics*, Vol. 14, No. 4, 1984, pp. 580–586.
- [32] Khatib, O., "Dynamic Control of Manipulators in Operational Space," *Proceedings of the Sixth World Congress on Theory of Machines and Mechanisms*, Wiley, New Delhi, India, 1983, pp. 1128–1131.

- [33] English, J. D., Maciejewski, A. A., "On the Implementation of Velocity Control for Kinematically Redundant Manipulators," *IEEE Transactions on Systems, Man, and Cybernetics, Part A: Systems and Humans*, Vol. 30, No. 3, 2000, pp. 233–237.
doi:10.1109/3468.844350
- [34] Papadopoulos, E., and Dubowsky, S., "On the Nature of Control Algorithms for Free-Floating Space Manipulators," *IEEE Transactions on Robotics and Automation*, Vol. 7, No. 6, 1991, pp. 750–758.
doi:10.1109/70.105384
- [35] Zhu, Y., and Li, X. R., "Recursive Least Squares with Linear Constraints," *Proceedings of the 38th IEEE Conference on Decision and Control*, Vol. 3, Phoenix, AZ, IEEE Publ., Piscataway, NJ, 1999, pp. 2414–2419.
- [36] Park, K. C., Chang, P. H., and Kim, S. H., "The Enhanced Compact QP Method for Redundant Manipulators Using Practical Inequality Constraints," *Proceedings of the 1998 IEEE International Conference on Robotics and Automation*, Vol. 1, Leuven, Belgium, IEEE Publ., Piscataway, NJ, 1998, pp. 107–114.
- [37] Cheng, F. T., Sheu, R. J., and Chen, T. H., "The Improved Compact QP Method for Resolving Manipulator Redundancy," *IEEE Transactions on Systems, Man, and Cybernetics*, Vol. 25, No. 11, 1995, pp. 1521–1530.
doi:10.1109/21.467718
- [38] Cheng, F. T., Chen, T. H., and Sun, Y. Y., "Resolving Manipulator Redundancy Under Inequality Constraints," *IEEE Transactions on Robotics and Automation*, Vol. 10, No. 1, 1994, pp. 65–71.
doi:10.1109/70.285587
- [39] Zhang, Y., and Ma, S., "Minimum-Energy Redundancy Resolution of Robot Manipulators Unified by Quadratic Programming and its Online Solution," *Proceedings of the 2007 IEEE International Conference of Mechatronics and Automation*, Harbin, China, IEEE Publ., Piscataway, NJ, 2007, pp. 3232–3237.
- [40] Zhang, Y., and Wang, J., "A Dual Neural Network for Convex Quadratic Programming Subject to Linear Equality and Inequality Constraints," *Physics Letters A*, Vol. 298, 2002, pp. 271–278.
doi:10.1016/S0375-9601(02)00424-3
- [41] Zhang, Y., Wang, J., and Xia, Y., "A Dual Neural Network for Redundancy Resolution of Kinematically Redundant Manipulators Subject to Joint Limits and Joint Velocity Limits," *IEEE Transactions on Neural Networks*, Vol. 14, No. 3, 2003, pp. 658–667.
doi:10.1109/TNN.2003.810607
- [42] Lawson, C. L., and Hanson, R. J., *Solving Least Squares Problems*, Prentice-Hall, Englewood Cliffs, NJ, 1974, pp. 134–173.
- [43] Van Loan, C., "On the Method of Weighting for Equality-Constrained Least-Squares Problems," *SIAM Journal on Numerical Analysis*, Vol. 22, No. 5, 1985, pp. 851–864.
doi:10.1137/0722051
- [44] Stewart, G. W., "On the Weighting Method for Least Squares Problems with Linear Equality Constraints," *BIT Numerical Mathematics*, Vol. 37, No. 4, 1997, pp. 961–967.
doi:10.1007/BF02510363
- [45] Yoshida, K., "Practical Coordination Control Between Satellite Attitude and Manipulator Reaction Dynamics Based on Computed Momentum Concept," *Proceedings of the IEEE/RSJ/GI International Conference on Intelligent Robots and Systems*, Vol. 3, Munich, Germany, IEEE Publ., Piscataway, NJ, 1994, pp. 1578–1585.
doi:10.1109/IROS.1994.407645
- [46] Longman, R., Lindberg, R., and Zedd, M., "Satellite-Mounted Robot Manipulators—New Kinematics and Reaction Moment Compensation," *The International Journal of Robotics Research*, Vol. 6, No. 3, 1987, pp. 87–103.
- [47] Hughes, P. C., *Spacecraft Attitude Dynamics*, Dover, New York, 2004, pp. 97–138.
- [48] Chung, C. L., and Desa, S., "A Global Approach for Using Kinematic Redundancy to Minimize Base Reactions of Manipulators," NASA CR-186825, March 1989.
- [49] Umetani, Y., and Yoshida, K., "Resolved Motion Rate Control of Space Manipulators with Generalized Jacobian Matrix," *IEEE Transactions on Robotics and Automation*, Vol. 5, No. 3, 1989, pp. 303–314.
doi:10.1109/70.34766
- [50] Nakamura, Y., Yokokohji, Y., Hanafusa, H., and Yoshikawa, T., "Unified Recursive Formulation of Kinematics and Dynamics of Robot Manipulators," *Proceedings of the Japan-USA Symposium on Flexible Automation*, Osaka, Japan, Japan Assoc. of Automatic Control Engineers Publ., Kyoto, Japan, 1986, pp. 53–60.
- [51] Rodriguez, G., Jain, A., and Kreutz-Delgado, K., "A Spatial Operator Algebra for Manipulator Modeling and Control," *The International Journal of Robotics Research*, Vol. 10, No. 4, 1991, pp. 371–381.
doi:10.1177/027836499101000406
- [52] Zhang, Y., and Wang, J., "Obstacle Avoidance for Kinematically Redundant Manipulators Using a Dual Neural Network," *IEEE Transactions on Systems, Man, and Cybernetics, Part B: Cybernetics*, Vol. 34, No. 1, 2004, pp. 752–759.
doi:10.1109/TSMCB.2003.811519
- [53] O'Neil, K. A., "Divergence of Linear Acceleration-Based Redundancy Resolution Schemes," *IEEE Transactions on Robotics and Automation*, Vol. 18, No. 4, 2002, pp. 625–631.
doi:10.1109/TRA.2002.801046
- [54] Park, J., Chung, W. K., and Youm, Y., "Characterization of Instability of Dynamic Control for Kinematically Redundant Manipulators," *Proceedings of the IEEE International Conference on Robotics and Automation*, Vol. 3, 2002, pp. 2400–2405.
- [55] Cocuzza, S., "Design and Construction of a Free-Flying 3D Robot for Space Applications and Microgravity Tests," Ph.D. Thesis, Center of Studies and Activities for Space "G. Colombo", Univ. of Padova, Padova, Italy, 2005.
- [56] Cocuzza, S., Bettanini, C., De Cecco, M., Menon, C., Zaccariotto, M., and Angrilli, F., "Free-Flying Robot 3D Simulator Validation by means of Air-Bearings Table 2D Tests—Test-Bed Design," 56th International Astronautical Congress, Fukuoka, Japan, International Astronautical Federation Paper IAC-05-C2.1.B.06, 2005.
- [57] Cocuzza, S., Menon, C., Aboudan, A., Bulgarelli, A., and Angrilli, F., "Free-Flying 3D Space Robot Prototype Design and Zero-G Experiments on ESA Parabolic Flights," 55th International Astronautical Congress, Vancouver, International Astronautical Federation Paper IAC-04-I.7.06, 2004.
- [58] Menon, C., Aboudan, A., Cocuzza, S., Bulgarelli, A., and Angrilli, F., "Free-Flying Robot Tested on Parabolic Flights: Kinematic Control," *Journal of Guidance, Control, and Dynamics*, Vol. 28, No. 4, 2005, pp. 623–630.
doi:10.2514/1.8498
- [59] Menon, C., Aboudan, A., Cocuzza, S., Bulgarelli, A., Bettanini, C., Marchesi, M., and Angrilli, F., "Self-Balancing Free Flying 3D Underactuated Robot for Zero-g Object Capture," 54th International Astronautical Congress, Bremen, Germany, International Astronautical Federation Paper IAC-03-J.2.06, 2003.
- [60] Cocuzza, S., Menon, C., and Angrilli, F., "Free-Flying Robot Tested on ESA Parabolic Flights: Simulated Microgravity Tests and Simulator Validation," 58th International Astronautical Congress, Hyderabad, India, International Astronautical Federation Paper IAC-07-A2.5.07, 2007.